Research Article

Peng Zhang, Xiaoyao Sun, Jiandong Wei, Juan Wang, and Zhen Gao*

Influence of PVA fibers on the durability of cementitious composites under the wet–heat–salt coupling environment

https://doi.org/10.1515/rams-2023-0155
received July 22, 2023; accepted November 16, 2023

Abstract: To investigate the effects of wet–heat–salt coupling environment (WHSCE) and the content of polyvinyl alcohol (PVA) fibers on the durability of cementitious composites (CC), a series of durability tests were carried out. In this study, the salt concentration in the WHSCE was set to 5%, the temperature at 50°C, and the relative humidity at 100%. Six different contents of PVA fibers were set up in the test for exploring their effects on the durability (impermeability, chloride ion penetration resistance, freeze–thaw resistance, and chloride salt erosion resistance under dry and wet cycle conditions) of CC. The results showed that durability of CC under the WHSCE was enhanced regardless of the content of PVA fibers added. At the PVA fiber amount of 1.2%, the impermeability pressure, electric flux, mass loss rate, compressive strength loss rate, and compressive strength corrosion resistance coefficient under the WHSCE reached the optimal values. This indicated that the durability of CC was most favorable when the amount of PVA fibers was 1.2% since many engineering structures are subject to erosion by various factors in the ocean, which can inevitably affect the service life of the purchase. In this study, the effect of PVA fiber content on the durability of CC in complex environment is studied, which provides experimental data and analytical ideas for improving engineering located in the ocean, hoping to provide a theoretical basis for their subsequent application in practical engineering.

Keywords: durability, cementitious composites, wet–heat–salt coupling environment

*** Corresponding author: Zhen Gao**, School of Water Conservancy and Transportation, Zhengzhou University, Zhengzhou, 450001, China, e-mail: gz12faafr@126.com
Peng Zhang, **Xiaoyao Sun**, **Jiandong Wei**, **Juan Wang:** School of Water Conservancy and Transportation, Zhengzhou University, Zhengzhou, 450001, China

1 Introduction

Concrete is used in the construction industry and exhibits the advantages of high strength, excellent plasticity, and easy access to materials, providing safe places to live for people around the world [1–3]. Concrete has been used for more than 200 years, but engineering is more concerned about mechanical properties than durability in the past. In fact, the service life of the engineering structures and the ability to operate effectively are determined by the durability [4]. As the aging problem of buildings becomes more and more serious, its durability is also getting more and more attention. Generally speaking, the degradation of the durability of concrete is related to the formation and development of cracks. When cracks appear, they accelerate the rate of transport of harmful ions such as chloride ions, leading to a decrease in the durability of the concrete structure, which in turn affects the safety of the structure [5,6]. It is well known that most of the engineering structures are in complex environments, resulting in concrete structures that are often subjected to a combination of temperature, high humidity, and high salt erosion [7,8]. This undoubtedly accelerates the formation of cracks.

In order to figure out the deterioration process and principles of cementitious composites (CCs) in different environments, many researchers have done a good deal of research. When CC is exposed to chloride solutions, some of the chlorides enter the material through the pores for free transport [9]. As a result, the compressive, tensile, and flexural strength properties of CC are reduced to varying degrees [10]. It has been demonstrated that the rate of chloride ion transport can be impacted by several elements – for instance, the pore structure properties of concrete itself, the chemical composition inside the pore solution, and the binding capacity of the chloride ions themselves [11]. Exposure to different salt solutions can also result in different chloride binding patterns. When exposed to sodium chloride solution, it is widely believed by domestic and foreign scholars that the Friedel salt

(C_3A–$CaCl_2$–$10H_2O$) is formed due to the association of $3CaO$–Al_2O_3 (C_3A) with chlorine ions through chemical binding. However, more chlorides are adsorbed on calcium silicate hydrate (C–S–H) by physical binding when exposed to $CaCl_2$ solution. The role of physical adsorption is relatively minor compared to chemical binding methods, but it is also particularly significant because of the high number of C–S–H gels. The higher number of bound chloride ions reduces the content of free chloride ions and thus reduces the possibility of erosion of the reinforcement [9,11–14].

Due to the complex climate around the world, concrete is also susceptible to high temperature and high humidity in addition to the high-salt environment. With the increase in temperature from 200 to 800°C, hydration products decomposed continuously and the appearance of concrete changed from light gray to slightly yellow to grayish brown and finally grayish white, accompanied by the appearance of microcracks [15]. When cracks were formed, they inevitably had a negative effect on the properties of concrete. As the temperature continued to rise, the weight loss of the specimen increased due to the evaporation of water from within the concrete and the spalling of the concrete. The compressive strength and modulus of elasticity of concrete in high-temperature environments were reduced to varying degrees [16,17]. At the same time, high temperatures may lead to brittle failure of CC and reduce strain-hardening properties [18]. The results of a number of studies have already shown that temperature variations are sensitive to the effects of tensile behavior [19,20]. The humid and hot geological environments are distributed all over the world. Both temperature and humidity are high in the construction of underground works such as tunnels. A hygrothermal environment is defined as a construction where the temperature is greater than or equal to 50°C and the humidity is greater than or equal to 80% and where the underground environment is greater than or equal to 30°C and the humidity is greater than or equal to 60°C [21]. The results of numerous studies have shown that concrete erosion is more severe when it is subjected to the action of wet–heat–salt coupling environment (WHSCE).

Compared to natural conditions, salt erosion is more corrosive to concrete materials under the action of dry and wet (D–W) cycles. It is obvious that the strength grows in the early stages owing to the hydration of concrete and the penetration of salts when concrete is subjected to the combined action of both [22]. As the number of D–W cycles continues to increase, the damage to the concrete is also increasing. As a consequence, the relative dynamic modulus of elasticity of concrete shows a trend of decreasing. Zhang *et al.* studied the resistance of CC to chloride salt erosion by simulating marine tidal environment. It was found that the content of free chloride ions increased with the increased exposure time [23]. A similar study was carried out by Li *et al.* [24]. The variable of temperature was added to the experiment. It was found that the movement of chloride ions accelerated as the temperature increased, which also led to the formation of cracks, thus hastening the transport of chloride ions in the cementitious material.

Fibers can improve the durability of CC [25]. For instance, the strength loss of concrete can be reduced by using glass beads as well as steel and polypropylene fibers [26], where steel and polypropylene fibers can also reduce porosity and thus improve durability [21]. It has also been demonstrated that the presence of fibers has a beneficial influence on both strength and crack development [27–29]. In summary, the inclusion of fibers can be seen to have a good enhancing effect on the durability of concrete. This may be due to the fact that fiber-reinforced concrete allows the CC to have a uniform distribution of reinforcing components in all directions. In general, fibers can be classified as natural and synthetic fibers [30]. Since the fibers themselves exhibit good toughness and high aspect ratio, they can be used as a reinforcing material for CC to diminish the generation of cracks and also to strengthen the performance of concrete after cracking [31]. A great deal of research has been conducted on the incorporation of fibers in CC. These results show that different types of fibers have their own characteristics. Basalt fibers are more inclusive of temperature and have good acid resistance [32]. They can also enhance the toughness and impact resistance [33]. Nevertheless, tensile strength and elasticity modulus are quite at a low level [34]. When 2% steel fibers were added to the engineered CC, the compressive strength and flexural strength increased by approximately 11 and 23.9%, respectively [10]. However, it causes the concrete to become unstable and rusty, accelerating the rate of steel consumption [35]. In view of this, many scholars have performed studies on polyvinyl alcohol (PVA) fibers as additives to enhance the durability.

PVA fibers have advantages of lower cost, better acid and alkali resistance, higher corrosion resistance, as well as a high modulus of elasticity. PVA fibers can form a mesh structure inside the concrete, making it less likely to crack when subjected to external forces [36,37]. Two of the more prominent advantages of PVA fibers are high tensile strength and good dispersibility [38–40]. The investigation results demonstrated that the splitting tensile strength of concrete increased by 4–7% when 0.2% PVA fiber was added [39]. Drying shrinkage performance is also an important performance of concrete. When PVA fibers are added, the cementitious material is more strongly bonded to the PVA fibers, and

the fibers inhibit shrinkage by shearing along the fiber–matrix interface [41,42]. Based on this principle, it is believed that the drying shrinkage strain of concrete decreases as the PVA fiber admixture increases [39,43]. As it is known, fibers can effectively limit the development of cracks. Therefore, the resistance to chloride ion penetration can also be improved by adding PVA fibers. However, when the content of PVA fibers is excessive, an agglomeration effect occurs and the bond between matrix and fibers may be weakened, resulting in the formation of cracks, which in turn increases the risk of chloride ion entry and destroys the durability.

At present, there are plenty of studies on the impact of PVA fibers on the durability of CC under the single action of humidity, temperature, and salt or the synergistic action of both. But many engineering is in more complex engineering environments, and there are a few studies on the effects of coupling multiple environmental factors on durability. Furthermore, the research of PVA fibers on durability under the coupling effect of multiple factors is even less. In order to overcome this shortcoming of the existing literature, this study focuses on the effect of PVA fiber content on the durability of CC in complex environments. The purpose of this study is to analyze the mechanism of damage to durability of CC by the WHSCE and the influence of PVA fiber on durability of CC in the WHSCE. When PVA fiber is added, the stress–strain properties of the matrix are improved and self-healing can occur, which greatly improves the durability of CC. By adding PVA fiber, the durability of CC in the WHSCE is improved, which is helpful to the study of the durability of CC under multi-factor coupling environment, and will help to explore an effective method to extend the service life of CC in complex environments.

2 Experiments

2.1 Materials

In this work, P·O 42.5 cement with a 28 day strength of 54.5 MPa was used. The performances of cement are presented in Table 1. The fly ash used in this test was manufactured by Luoyang Power Plant, and its physical properties are demonstrated in Table 2. The aggregate used in this test was extra-fine quartz sand material with a particle size range of 75–120 μm, and PVA fibers were supplied by Kuraray Company of Japan. Table 3 displays the detailed performances of PVA fibers. In this experiment, the water reduction rate of polycarboxylic acid with high-efficiency water reducer used was 25%.

2.2 Mix proportions

In accordance with the experimental studies of PVA-reinforced CC by present scholars [44,45], six volume contents (0, 0.3, 0.6, 0.9, 1.2, and 1.5%) of PVA fibers were set up. In this study, the water–binder ratio was set to 0.35 and the binder–sand ratio was set to 2. In addition, the mass of fly ash accounted for 35% of the total mass of the cementitious material. To investigate the effect of PVA fiber on durability of CC under the WHSCE, the mix proportioning of CC is demonstrated in Table 4, where M-0 indicates the

Table 1: Performances of cement

Specific surface area ($m^2 \cdot kg^{-1}$)	Setting time (min)		Compressive strength (MPa)		Flexural strength (MPa)	
	Initial setting	Final setting	3 days	28 days	3 days	28 days
386	90	300	26.6	54.5	5.42	8.74

Table 2: Technical specifications of fly ash

Test content	Water absorption (%)	Density ($g \cdot cm^{-3}$)	Standard consistency (%)	Stacking density ($g \cdot cm^{-3}$)
Average value	106	2.16	47.1	0.77

Table 3: Performances of PVA fibers

Diameter (μm)	Elongation (%)	Standard length (mm)	Tensile strength (MPa)	Young's modulus (GPa)
40	6.5	12	1,560	42

Table 4: Mix properties of each type of specimen

No.	Water ($kg \cdot m^{-3}$)	Fly ash ($kg \cdot m^{-3}$)	Cement ($kg \cdot m^{-3}$)	Quartz sand ($kg \cdot m^{-3}$)	PVA fiber (%)	Water reducer ($kg \cdot m^{-3}$)
M-0	350	350	650	500	0	1.5
M-1	350	350	650	500	0	1.5
P-0.3	350	350	650	500	0.3	2.0
P-0.6	350	350	650	500	0.6	2.5
P-0.9	350	350	650	500	0.9	3.0
P-1.2	350	350	650	500	1.2	3.5
P-1.5	350	350	650	500	1.5	4.0

specimens without PVA fiber and under natural environment, M-1 indicates the specimens without PVA fiber but under the WHSCE, P stands for PVA fiber, and the subsequent number represents the PVA fiber content.

2.3 Mixture preparation

In order to prepare PVA-reinforced CC with excellent durability, it is essential to ensure a more uniform dispersion of PVA fibers in the matrix. Therefore, the PVA fibers ought to be added in several times during blending process. First, fly ash, cement, and fine aggregate were stirred for 2 min. In the next step, some of the water and water-reducing agent were added and continued mixing for 2 min. Then, the remaining water was added and stirred for 1 min. Finally, the PVA fibers were incorporated into the mixer in four times and stirred for a total of 4 min to form the specimen. The specific process is illustrated in Figure 1.

2.4 Test methods

2.4.1 Simulation of WHSCE

The test simulated the WHSCE by varying the environmental variables. In this study, the TR-WSYP-31 was to simulate coupling environment, as presented in Figure 2. It had an inner chamber size of 3,000 × 4,000 × 2,100 mm. There were air ducts with four air blowers at the back side of the chamber. In addition, rain spray pipes were arranged on the top to meet the requirement of rainfall function. Salt spray nozzles were arranged on both sides, and a total of four nozzles were arranged to realize the requirement of spray function. The refrigeration system was installed outside the room, and the refrigeration machine adopted German Bock semi-closed compressor. Insulation material adopted polyurethane foam. And there are two silicone rubber door seals with good sealing performance.

It was found that the construction temperature of tunnels and other underground works and the actual service temperature of bridges could reach up to 50°C. In addition, the temperature in the range of 50–100°C could effectively improve the interfacial properties of the fiber and the matrix. Since the marine engineering was located in a

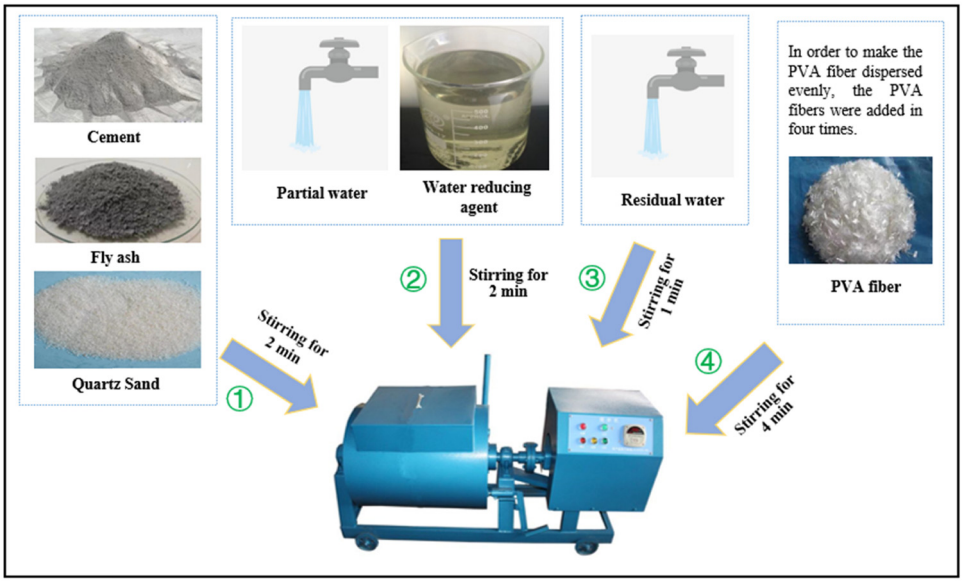

Figure 1: Process diagram for preparing CC.

(a) (b)

Figure 2: Environmental simulation test chamber: (a) appearance of the test chamber and (b) inside of the test chamber.

humid environment, the temperature of this environmental chamber was set to 50°C and the relative humidity to 100% considering the actual engineering and test conditions. The salt concentration in the simulated environment was 5% sodium chloride solution, and the degradation treatment time was 30 days. The values of salt concentration and degradation time referred to the salt concentration in the salt spray test method and the salt concentration and degradation time in the simulated artificial seawater tidal zone chlorine salt erosion test by Zhang *et al.* [23]. After the specimens were formed, they were placed in a cool indoor place, demolded after 24 h, and placed in a standard curing room (curing temperature of 20 ± 2°C and relative humidity of 95% or more) for 28 days.

2.4.2 Impermeability test

According to the JGJ/T 70-2009 [46], the dimensions of the specimens in the impermeability test were 70 mm in diameter at the top opening, 80 mm in diameter at the bottom, and 30 mm in height. After demolding, the specimen was placed in a standard curing room with a temperature of 20 ± 2°C for 28 days. After the curing, the specimen was taken out and placed in the natural environment for 45 days to conduct the simulation test of the WHSCE. After 30 days of the test, it was taken out and the impermeability was tested. The instrument used was mortar permeability meter produced by Shanghai Dongxing Building Materials Testing Equipment Co. By comparing the sealing effects of cement, paraffin, and silicone, neutral silicone adhesive was eventually chosen as the sealing material for the specimens in this test, which is shown in Figure 3, and applied to the side of the specimen with a thickness of about 5 mm. The instrument used to analyze the pore structure was a high-performance automatic mercury pressure meter. Figure 4 shows the water penetration of the specimens when the sealing material is silicone. When water seepage occurred at the end face of three of the six specimens, the test could be stopped and the water pressure was recorded at that time.

Figure 3: Silicone structural adhesive.

Figure 4: Sealing materials for silicone water penetration of the specimen.

The impermeability pressure values were calculated as follows:

$$P = H - 0.1, \tag{1}$$

where P represents the impermeability pressure of mortar (MPa) and H is the water pressure during water seepage in three of the six specimens (MPa).

2.4.3 Chloride ion penetration test

According to the Chinese standard GBT50082-2009 [47], the chloride ion penetration resistance was represented by the electric flux method. In this study, the CABR-RCP9-type concrete chloride ion electric flux tester was used, as shown in Figure 5. The specimen was a cylinder with a diameter of 100 mm and a height of 50 mm. Before the start of the test, the treatment method was the same as that of the impermeability test. The difference was that the surface or side of the specimen should be coated with silicone or resin sealing material. The specimen was then filled with water under vacuum. The specific steps were first to put the specimen into a vacuum container, and the absolute pressure in the vacuum container to 1–5 kPa within 5 min was reduced and maintained it for 3 h. Then, enough distilled water was injected under the condition of vacuum pump operation, and the specimen was immersed for 1 h and normal pressure was maintained. After drying, the relative humidity was kept above 95% and the specimen was installed in the test tank, as shown in Figure 6. After installation, the sealing performance between the specimen and the test tank should be checked using distilled water. After connecting the power line correctly, the power supply should be turned on with a constant voltage of 60 ± 0.1 V DC applied to both poles while keeping the test tank full of the solution. The instrument should be energized for at least 6 h, and it automatically records the electric flux value for each time period. The total columbic flux of each specimen is expressed by the following simplified equation:

$$Q_x = 900(I_0 + 2I_{30} + 2I_{60} + \cdots + 2I_t + \cdots + 2I_{300} + 2I_{330} + 2I_{360}), \tag{2}$$

where Q_x is the total columbic electric flux through sample (C), I_0 is the initial current (A), and I_t is the current at t time (A).

The calculation should be converted according to the following formula:

$$Q_s = Q_x \times \left(\frac{95}{x}\right)^2, \tag{3}$$

where x represents the actual diameter of the samples (mm) and Q_s stands for electric flux through samples with a diameter of 95 mm (C).

2.4.4 F–T cycle test

Based on JGJ/T 70-2009 [46], the rapid F–T cycle test was performed. Cubic specimen size was 70.7 × 70.7 × 70.7 mm. After the end of the role of the WHSCE, the specimens were taken out and dried and then soaked in water at 15–20°C for 2 days. Afterward, the surface water was wiped off and the mass was weighed. The specimens were put into the test box with a net cross-section of 120 × 120 × 500 mm when they were filled with water and then put them into the F–T machine. The test box with the temperature test specimen was placed in the center of the testing machine. The F–T medium was used as antifreeze solution for the temperature test specimen, and the temperature sensor was inserted into the temperature test specimen and

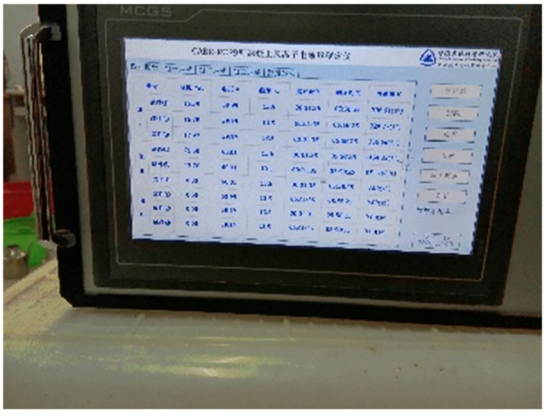

Figure 5: Chloride ion flux tester.

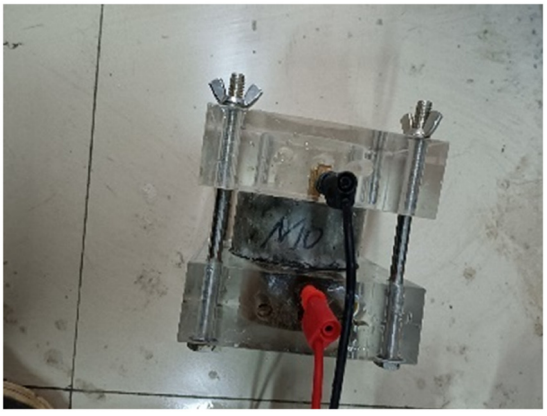

Figure 6: M-0 specimen mounted in the test tank.

antifreeze solution, respectively. The time to complete each F–T cycle was 2–4 h. At the end of F–T cycle, the central temperature of the sample was supposed to be controlled within −17 ± 2°C and 8 ± 2°C, respectively. After each 25 cycles, samples need to be tested for compressive strength and mass loss. Figure 7 shows the state of M-0 specimens before and after F–T cycles, from which it can be seen that the specimen has been subjected to the phenomenon of spalling of the surface paste after F–T cycles as well as mass loss. The strength loss rate of the sample shall be calculated in accordance with the following formula:

$$\Delta f_n = \frac{f_0 - f_n}{f_0} \times 100\%, \tag{4}$$

where Δf_n is the mortar strength loss rate after n F–T cycles (%), f_0 is the average compressive strength of samples (MPa), and f_n is the average compressive strength of the three samples after n F–T cycles (MPa).

The mass loss rate after F–T cycles should be calculated according to the following formula:

$$\Delta m_n = \frac{m_0 - m_n}{m_0} \times 100\%, \tag{5}$$

where Δm_n represents the mass loss rate of samples after n F–T cycles (%), calculated by taking average value of three specimens; m_0 is the mass before F–T cycles (g), and m_n stands for the mass after n F–T cycles (g).

2.4.5 Chlorine salt erosion resistance test under D–W cycle conditions

Cubic samples with dimensions of 100 × 100 × 100 mm were used in this experiment. The specimens to be subjected to D–W cycles were removed from the simulation chamber and dried at 80 ± 5°C for 48 h. After drying, the specimen was cooled to room temperature. The specimen was placed in a box containing 5% sodium chloride solution and placed in a simulated environment box for temperature control. After soaking in sodium chloride solution for 12 h, the sample was removed from the solution and dried at high temperature for 12 h. This cycle was repeated until 30 cycles were completed and repeated every 15 cycles. The sodium chloride solution was replaced after every 15 D–W cycles. After 30 D–W cycles, the chloride erosion process was complete as shown in Figure 8. At the end of the process, the specimen was taken out, the surface of the specimen was observed, and the compressive strength of the specimen was tested. The compressive strength corrosion resistance coefficient is used to reflect chlorine salt erosion resistance, which is calculated in the following equation:

$$K_{cf} = \frac{f_{cn}}{f_{c0}}, \tag{6}$$

where K_{cf} represents the compressive strength corrosion resistance factor (%), f_{cn} is the measured value of compressive strength of a group of mortar specimens subjected to chloride salt corrosion after n D–W cycles (MPa), f_{c0} represents the measured compressive strength of a set of comparative CC specimens at the same age as the specimens subjected to chloride salt corrosion with standard curing (MPa).

2.4.6 Scanning electron microscope (SEM)

Selected specimens from CC after 125 F–T cycles were subjected to microscopic observation by SEM test. The impacts

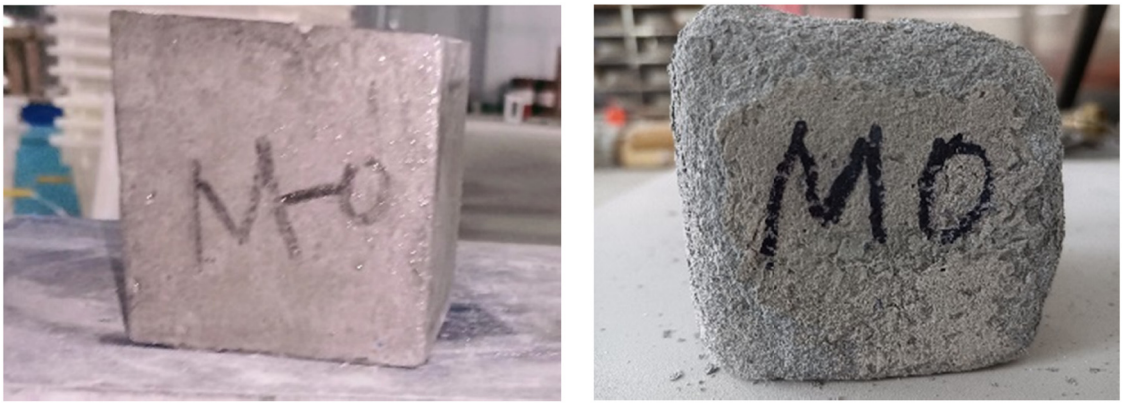

Figure 7: Before and after F–T cycles of M-0 specimen: (a) before F–T cycle and (b) after F–T cycle.

Figure 8: Compressive strength test of specimens after 30 D–W cycles.

of F–T cycles and PVA fibers on the microstructure of CC under the action of WHSCE were analyzed.

3 Results and discussion

3.1 Impermeability

Impermeability can indicate the resistance of concrete to attack by externally occurring substances. Figure 9 illustrates the impact of PVA fiber admixture on the impermeability pressure of CC under the WHSCE. It is evident that impermeability pressure of the control group samples under the action of the WHSCE reduced by 42.1% to that of the samples under natural environment. This is mainly because the higher temperature, humidity, and salt concentration in the WHSCE can accelerate the transport of chloride ion in the CC, causing the chloride salt to generate a large amount of Friedel salt and Kuzel salt. This leads to fine cracks and larger pores in the matrix. With the increase in the number of cracks and the development of pores, the penetration of water into the matrix is accelerated, thus reducing its impermeability. The impermeability pressure of CC under the WHSCE showed a tendency to increase initially and decrease later as PVA fiber content increased. With increasing the amount of PVA fibers from 0.3 to 1.2%, impermeability pressure under the action of the WHSCE increased by 33.3, 66.7, 100, and 166.7%, respectively, in comparison with those of control group under the natural environment. However, the impermeability pressure decreased as the PVA fiber content continued to increase to 1.5%. This may be due to the disordered distribution of PVA fibers in the CC under the WHSCE, which can form a perfect support system and prevent the matrix from cracking [48]. At the same time, the denseness is improved and the pores are reduced, thus improving the impermeability of the matrix [49]. But excessive PVA fibers are not uniformly distributed in the matrix and tend to agglomerate. This causes an increase in porosity, resulting in a reduction in impermeability of matrix [50].

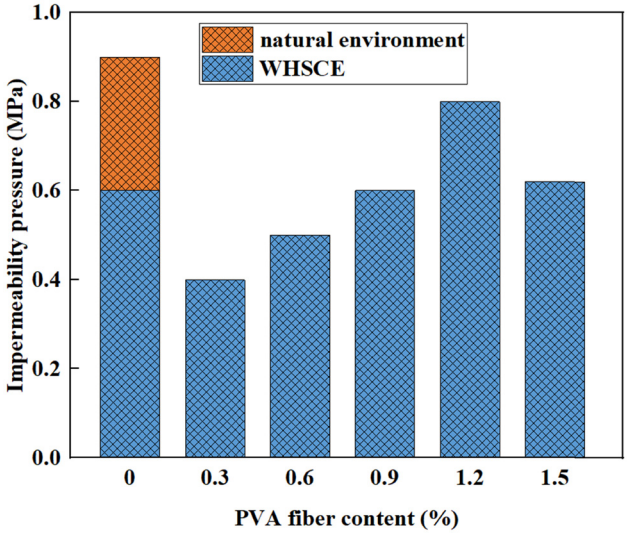

Figure 9: Impact of PVA fiber content on impermeability pressure.

Cracks are prone to appear near the pores [51]. And the mechanical properties and durability of CC are also affected by pores [52,53]. The pore content can be characterized by porosity, while the pore volume ratio can visualize the distribution of the volume of various types of pores. The effects of WHSCE and PVA fibers on the pore size and porosity of the CC were investigated by mercury intrusion porosimetry. As seen in Figure 10, the number of the multi-harmful pores (200 nm to 1 μm) and capillary pores (>1 μm) increases in the CC under the WHSCE, while the number of less hazardous pores (<50 nm and 50–200 nm) decreases significantly. This indicated that WHSCE changed the distribution of the number of each pore size, and the increase in the porosity of larger pores was more obvious. In contrast, an incorporation of PVA fibers in CC under the action of WHSCE increased the number of less harmful pore in the matrix and was higher than the control group. As PVA fibers were added, the amount of multi-harmful and capillary

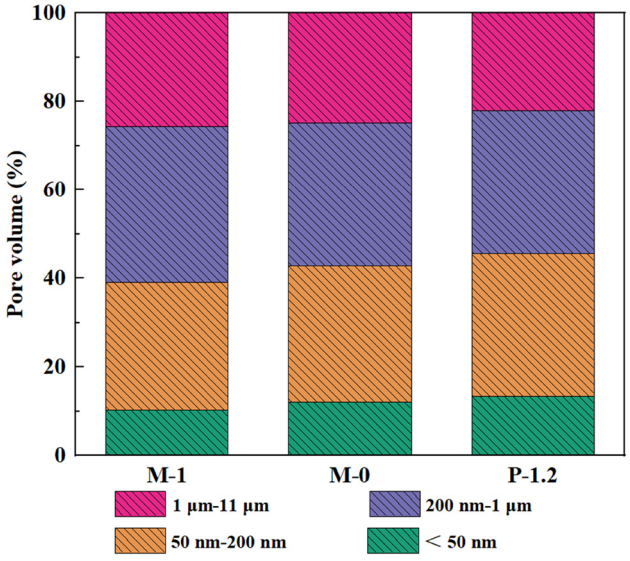

Figure 10: Effect of WHSCE and 1.2% PVA fibers on pore volume.

pores of CC decreased. This is also the reason why the impermeability of the matrix is improved [54].

It can be visualized from Figure 11 that the porosity of CC under natural environment is 14.23%, while it increases more significantly to 18.36% under the action of the WHSCE. However, the porosity decreased significantly to 10.6% after adding 1.2% PVA fibers. This may be explained by the fact that the high temperature and salt in the WHSCE can make the CC more microporous to the extent that the deleterious pore volume ratio, capillary pore volume ratio, and porosity in the matrix are increased [55]. Nevertheless, once PVA fibers are added, they can bond more firmly with the CC due to their smaller radii and the hydrocarbon groups in the fibers. The hydration enhancement of PVA fibers produces more C–S–H gels, resulting in a more compact structure [56]. Therefore, the incorporation of PVA fibers improved compactness, which in turn reduced the porosity in the matrix and effectively improved the pore structure.

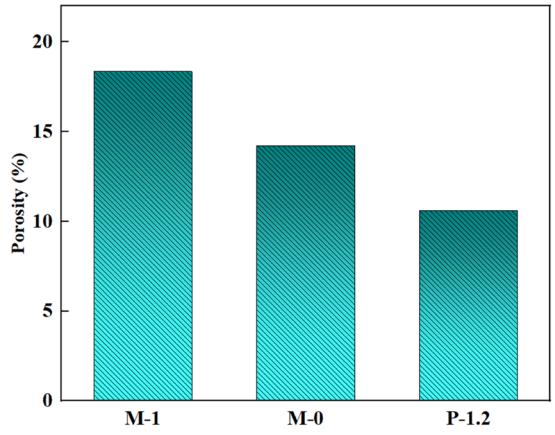

Figure 11: Effect of WHSCE and 1.2% PVA fibers on porosity.

3.2 Chloride penetration resistance

It is well known that many buildings are subject to marine erosion, which shortens their service life. In contrast, polymer fibers are less susceptible to chloride and salt erosion [57]. Therefore, in this study, PVA fibers were incorporated into CC to investigate chloride ion penetration resistance in CC under WHSCE. As can be seen in Figure 12, the electric flux of the CC increased by 4.66% in the WHSCE compared to the control group. This is largely owing to an increase in microcracks within specimens under the WHSCE. Moreover, the salt ions produce more chloride ions that have an erosive effect on the matrix. Each of these increases the electric flux values of the CC and reduces chloride ion penetration resistance of the matrix [58].

The electric flux value showed a trend of first decreasing and then increasing under the action of the WHSCE as PVA fiber content increased. When the content of PVA fibers increased from 0.3 to 1.2%, the electric flux values decreased by 16.76, 20.91, 24.20, and 28.6% compared with those of CC without PVA fiber. However, when the PVA fiber admixture continued to increase to 1.5%, the electrical flux value of the CC increased by 15.7% compared to the matrix admixed with 1.2% PVA fiber. Nevertheless, the electric flux decreased by 17.4% compared to the CC without PVA fiber. This indicated that the 1.5% PVA content still had an enhanced effect on the chloride penetration resistance. The reasons for this

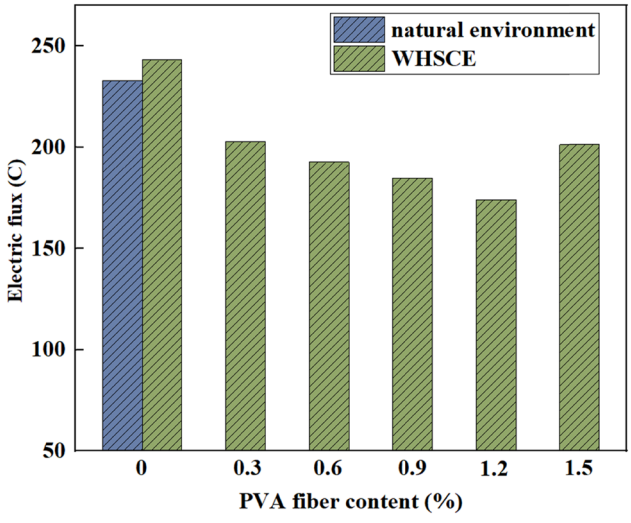

Figure 12: Influence of PVA fiber content on electric flux.

experimental result are similar to those for impermeability. The appropriate amount of PVA fibers can be uniformly distributed in the CC [59], reducing the number of cracks in the matrix. However, the excessive incorporation of PVA fibers in CC tends to form the agglomeration effect. Moreover, the mixing process of adding PVA fibers introduces microbubbles, which increases the porosity of CC and thus reduces the chloride ion permeability of CC in a WHSCE [60].

3.3 F–T resistance

The damage of F–T cycles is the main disease in hydraulic concrete structures. On the one hand, it can reduce the durability of CC. On the other hand, the cost of later maintenance can be greatly increased. In general, the relative dynamic modulus of elasticity is a reflection of F–T resistance [61]. But in this study, the compressive strength loss rate and mass loss rate were used to reflect the F–T resistance of CC. Figures 13 and 14 show the relationship between the compressive strength loss rate and mass loss rate of CC and the number of F–T cycles, respectively. The compressive strength and mass loss rate under WHSCE are both significantly lower compared to the natural environment. This can be explained by the fact that more pores and cracks are more likely to be formed in CC under the action of the WHSCE, which reduces the F–T resistance of CC. The F–T cycle leads to the freezing of water in the CC, generating expansion pressure and leading to spalling of cement paste [62].

Furthermore, the compressive strength loss rate and mass loss rate of CC exhibited a tendency of initially decreasing and then increasing as the amount of PVA fibers was increased under the WHSCE. Figures 13 and 14 indicate that the compressive strength loss rate and mass loss rate gradually decrease with PVA fiber admixture increasing from 0 to 1.2% at the same number of F–T cycles. When the number of F–T cycles was 125, the compressive strength loss rate decreased by 10.06, 24.65, 39.35, and 47.99% with a PVA fiber content of 0.3, 0.6, 0.9, and 1.2%, respectively, compared with the specimens without PVA fiber. And the mass loss rate decreased by 6.73, 6.21, 6, 5.32, and 5.68%. However, the compressive strength loss rate of the specimens increased by 22.75% at a PVA fiber incorporation of 1.5%, compared with the specimens containing 1.2% PVA fiber. The mass loss rate also presented a rising trend. It is because high elastic modulus and high toughness of PVA fibers are able to play a bonding role to matrix, so it can be subjected to a larger expansion pressure, which can improve the frost resistance of the CC under the WHSCE [63]. In addition, PVA fibers can act as a bridge between microcracks and suppress the development of cracks [41]. Nevertheless, the incorporation of excessive PVA fibers may cause uneven compactness of the matrix, thus reducing the frost resistance of CC under the WHSCE.

3.4 Resistance to chlorine salt attack under D–W cycle conditions

Chlorine salt attack is another important cause of structural durability damage [23]. The results of the study show that chloride migration can be influenced not only by

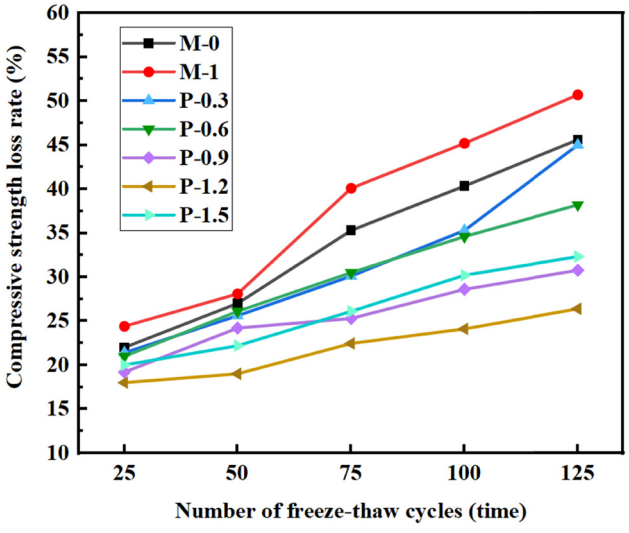

Figure 13: Effect of number of F–T cycles on comprehensive strength loss rate.

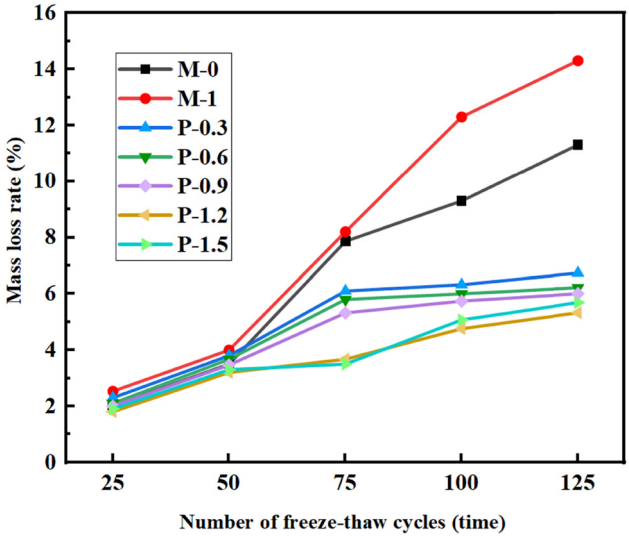

Figure 14: Influence of number of F–T cycles on mass loss rate.

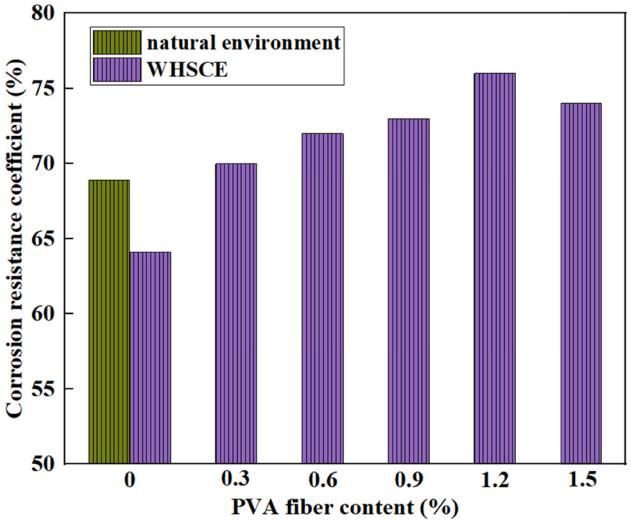

Figure 15: Influence of PVA fiber content on the compressive strength corrosion resistance coefficient.

electrochemical interactions in the C–S–H layer, but likewise by chemical interactions in anhydrous cements [64–66]. Generally speaking, the environment in which the building is located is complex, so it is desirable to investigate the performance of CC to resist chlorine salt attack under D–W cycle conditions. Figure 15 illustrates the impact of PVA fiber incorporation on the compressive strength corrosion coefficient of CC under the WHSCE. It was evident that the compressive strength corrosion coefficient of samples declined under D–W cycles without PVA fiber incorporation when compared with the control group. With an increase in the amount of PVA fibers from 0.3 to 1.2%, the compressive strength corrosion coefficient increased by 9.36, 12.31, 13.87, and 18.55%, respectively, compared with the control group. As the amount of PVA fibers proceeded to increase to 1.5%, the compressive strength corrosion coefficient decreased.

This showed that an appropriate dosage of PVA fibers in CC could improve the compressive strength corrosion coefficient of the matrix, which was due to the high tensile strength of PVA fibers. When PVA fibers are dispersed in the matrix, they can inhibit the generation of microcracks in CC through the bridging effect, which in turn can play a role in toughening and anti-cracking of CC [67]. Moreover,

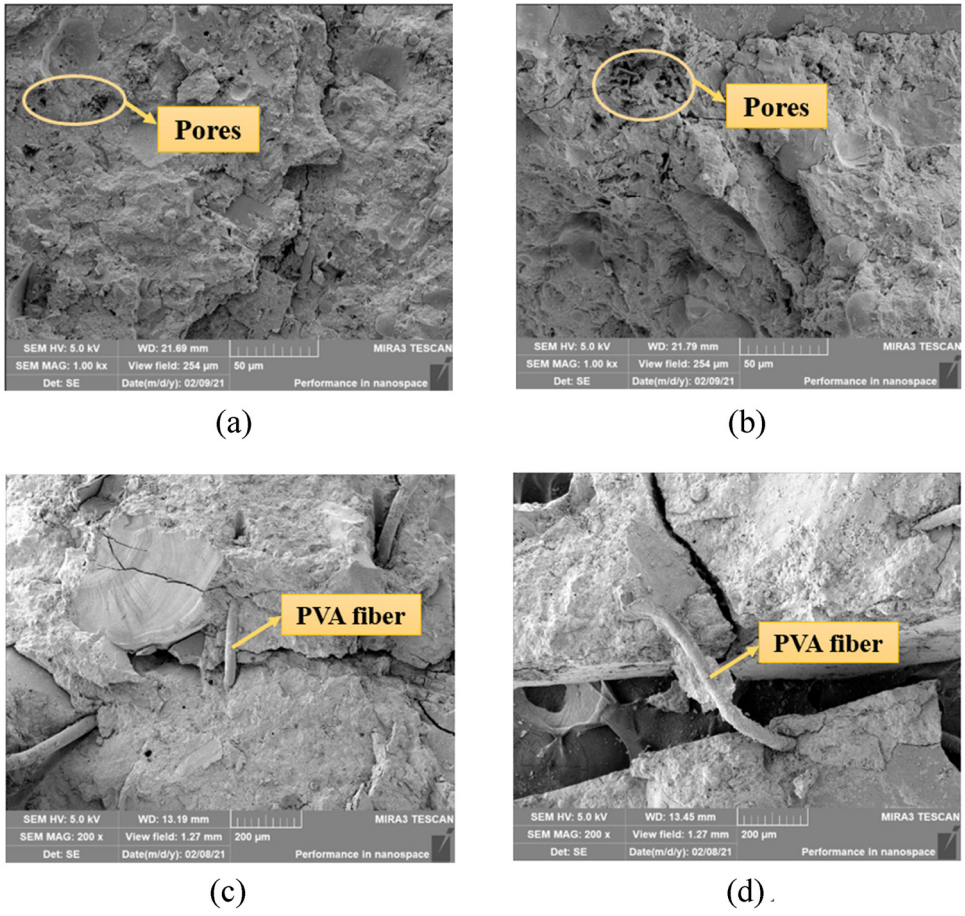

Figure 16: SEM images of CC: (a) after F–T cycle (M-0), (b) after F–T cycle (M-1), (c) before F–T cycle, and (d) after F–T cycle.

it can improve the performance of the interface transition zone. Accordingly, the compressive strength corrosion coefficient of matrix is improved. However, beyond a certain amount of admixture, the excess PVA fibers are not easily dispersed in the CC and tend to agglomerate, causing voids in the matrix, which in turn leads to weak points in the CC [45,68]. Furthermore, PVA fibers have the property of hydrophilicity. The PVA fibers can inhibit the hydration reaction in the matrix after water absorption, which results in a reduction of the compressive strength corrosion coefficient [69].

3.5 Microstructure

SEM is often used to test the properties of materials on the surface of a sample and is widely used in the field of scientific research. During the process of cement setting and hardening, cracks and voids inevitably appear at the interface between cement and aggregate due to water secretion, shrinkage, segregation, *etc*. These microcracks increase the deterioration points in the matrix of CC, and the microcracks and pores expand and connect under internal and external stresses, leading to the deterioration of the matrix microstructure and the worsening of the frost resistance [70]. Figure 16a and b shows the SEM images of CC without PVA fiber after F–T cycles, where samples in (a) are conditioned under natural environment and (b) is the SEM image of the specimen after the action of WHSCE. From Figure 16b, it can be seen that the small pores of the CC under the WHSCE are significantly increased. The surface of the CC was eroded under the synergistic actions of the WHSCE and F–T cycles. The capillary tension and the difference in solubility of the salt solution will cause osmotic pressure, which led to an increase in water absorption rate [71]. This is also the reason for the increase of small pores in (b).

Figure 16c and d demonstrates the SEM images of CC containing 1.2% PVA fiber before and after F–T cycles under the action of WHSCE, respectively, where the amount of F–T cycles was set at 125 in (d). Comparing (c) and (d), it was observed that F–T cycles not only increased the amount of cracks of CC, but also enlarged the width of cracks. However, PVA fibers are distributed chaotically in the matrix, whereby the formation of a mesh structure improves the compactness of the matrix. PVA fibers can bridge microscopic cracks in the cement matrix, prevent and inhibit material segregation, and also relieve the concentrated frost swelling stress and transmit the stress to the matrix, thus preventing further expansion of cracks [72]. However, it can still be seen from (d) that the bonding of PVA fibers to the matrix decreases, leading to a decrease in the strength of matrix at the end of F–T cycles.

4 Conclusions

In this study, it focused on the effect of PVA fiber amount on durability under the WHSCE. The main experiments were impermeability test, rapid chloride ion test, rapid F–T test, chloride salt erosion resistance test under D–W cycles, SEM test, and mercury intrusion porosimetry test, and the data of impermeability pressure value, electric flux value, compressive strength loss rate and mass loss rate, compressive strength corrosion resistance coefficient, and pore volume rate of CC were analyzed to do the compilation and analysis, and the following conclusions were drawn:

1) In comparison with the natural environment, the harmful pores and porosity of CC increased under the action of the WHSCE. The impermeability and chloride ion penetration resistance were reduced. The number of small pores in the matrix increased and the F–T resistance decreased.
2) As the PVA fiber content increased from 0.3% to 1.5%, the impermeability pressure of the matrix under the action of the WHSCE first increased and then decreased. When the PVA fiber content was 1.2%, the number of harmful pores and porosity of CC decreased to the lowest value and the impermeability pressure value of CC reached the maximum value of 0.8 MPa.
3) At a PVA fiber content of 1.2%, electric flux value of the CC under the action of the WHSCE decreased by 28.6%, and the resistance to chloride ion penetration was optimal. And the compressive strength corrosion resistance coefficient was increased by 18.55% than that in the control group, at which time chloride salt erosion resistance of CC under D–W cycles reached the best performance.
4) With the same number of F–T cycles, the compressive strength loss rate and mass loss rate of CC under the action of the WHSCE showed a trend of first decreasing and then increasing as the PVA fiber content increased. At the PVA fiber content of 1.2% and the times of 125 F–T cycles, compressive strength loss and mass loss reached the minimum value, which were 47.99 and 20.95% lower than those of the control group, respectively.

Acknowledgments: The authors would like to thank all the editors and the anonymous referees for their constructive comments and suggestions.

Funding information: The authors would like to acknowledge the financial support received from National Natural Science Foundation of China (Grant No. U2040224), Natural Science Foundation of Henan (Grant No. 232300421003), and Project Special Funding of Yellow River Laboratory (Grant No. YRL22LT02).

Author contributions: All authors have accepted responsibility for the entire content of this manuscript and approved its submission.

Conflict of interest: The authors state no conflict of interest.

References

[1] Gao, Y., B. Wang, C. Liu, D. Hui, Q. Xu, Q. Zhao, et al. Experimental investigation on static compressive toughness of steel fiber rubber concrete. *Reviews on Advanced Materials Science*, Vol. 61, 2022, pp. 576–586.

[2] Golewski, G. L. Study of strength and microstructure of a new sustainable concrete incorporating pozzolanic materials. *Structural Engineering and Mechanics*, Vol. 86, 2023, pp. 431–441.

[3] Golewski, G. L. Mechanical properties and brittleness of concrete made by combined fly ash, silica fume and nanosilica with ordinary Portland cement. *Aimsmates*, Vol. 10, 2023, pp. 390–404.

[4] Taffese, W. Z. and E. Sistonen. Machine learning for durability and service-life assessment of reinforced concrete structures: Recent advances and future directions. *Automation in Construction*, Vol. 77, 2017, pp. 1–14.

[5] Wang, C., P. Zhang, J. J. Guo, J. Wang, and T. H. Zhang. Durability and microstructure of cementitious composites under the complex environment: Synergistic effects of nano-SiO2 and polyvinyl alcohol fiber. *Construction and Building Materials*, Vol. 400, 2023, id. 132621.

[6] Zhang, P., P. Yuan, J. F. Guan, and J. J. Guo. Fracture behavior of multi-scale nano-SiO2 and polyvinyl alcohol fiber reinforced cementitious composites under the complex environments. *Theoretical and Applied Fracture Mechanics*, Vol. 122, 2022, id. 103584.

[7] Fu, Q., Y. Wu, N. Zhang, S. Hu, F. Yang, L. Lu, et al. Durability and mechanism of high-salt resistance concrete exposed to sewage-contaminated seawater. *Construction and Building Materials*, Vol. 257, 2020, id. 119534.

[8] Zheng, C. A. L., S. X. Li, Y. F. Hou, and B. H. Jin. Frost resistance of fiber-reinforced self-compacting recycled concrete. *Reviews on Advanced Materials Science*, Vol. 61, 2022, pp. 711–725.

[9] Machner, A., M. Zajac, M. Ben Haha, K. O. Kjellsen, M. R. Geiker, and K. De. Weerdt. Stability of the hydrate phase assemblage in Portland composite cements containing dolomite and metakaolin after leaching, carbonation, and chloride exposure. *Cement and Concrete Composites*, Vol. 89, 2018, pp. 89–106.

[10] Sridhar, R. Durability study on engineered cementitious composites with hybrid fibers under sulfate and chloride environments. *Cleaner Materials*, Vol. 5, 2022, id. 100121.

[11] Luo, D. M., F. Li, and G. H. Xing. Corrosion resistance of 6061-T6 aluminium alloy and its feasibility of near-surface reinforcements in concrete structure. *Reviews on Advanced Materials Science*, Vol. 61, 2022, pp. 638–653.

[12] Shi, Z., M. R. Geiker, K. De Weerdt, T. A. Østnor, B. Lothenbach, F. Winnefeld, et al. Role of calcium on chloride binding in hydrated Portland cement–metakaolin–limestone blends. *Cement and Concrete Research*, Vol. 95, 2017, pp. 205–216.

[13] De Weerdt, K., A. Colombo, L. Coppola, H. Justnes, and M. R. Geiker. Impact of the associated cation on chloride binding of Portland cement paste. *Cement and Concrete Research*, Vol. 68, 2015, pp. 196–202.

[14] Zhang, P., W. S. Wang, Y. J. Lv, Z. Gao, and S. Y. Dai. Effect of polymer coatings on the permeability and chloride ion penetration resistances of nano-particles and fibers-modified cementitious composites. *Polymers*, Vol. 14, 2022, No. 16, id. 3258.

[15] Xiao, L. L., P. H. Chen, J. S. Huang, S. Peng, and Z. Yang. Compressive behavior of reinforced steel-PVA hybrid fiber concrete short columns after high temperature exposure. *Construction and Building Materials*, Vol. 342, 2022, id. 127935.

[16] Pourfalah, S. Behaviour of engineered cementitious composites and hybrid engineered cementitious composites at high temperatures. *Construction and Building Materials*, Vol. 158, 2018, pp. 921–937.

[17] Zhang, P., X. Han, S. W. Hu, J. Wang, and T. Y. Wang. High-temperature behavior of polyvinyl alcohol fiber-reinforced metakaolin/fly ash-based geopolymer mortar. *Composites Part B – Engineering*, Vol. 244, 2022, id. 110171.

[18] Mechtcherine, V., F. de, A. Silva, S. Müller, P. Jun, and R. D. T. Filho. Coupled strain rate and temperature effects on the tensile behavior of strain-hardening cement-based composites (SHCC) with PVA fibers. *Cement and Concrete Research*, Vol. 42, 2012, pp. 1417–1427.

[19] Çavdar, A. The effects of high temperature on mechanical properties of cementitious composites reinforced with polymeric fibers. *Composites Part B: Engineering*, Vol. 45, 2013, pp. 78–88.

[20] Zhang, P., Q. Y. Han, J. J. Wu, and Y. Zhang. Mechanical properties of nano-SiO2 reinforced engineered cementitious composites after exposure to high temperatures. *Construction and Building Materials*, Vol. 356, 2022, id. 129123.

[21] Lv, J. D. and L. C. Zhao. Effect of composite fiber and vitrified beads on the performance of concrete in hot-humid environment. *China Concrete and Cement Products*, Vol. 304, 2021, pp. 54–58.

[22] Zhang, P., Y. W. Sun, J. D. Wei, and T. H. Zhang. Research progress on properties of cement-based composites incorporating graphene oxide. *Reviews on Advanced Materials Science*, Vol. 62, 2023, id. 20220329.

[23] Zhang, P., Z. J. Zhuang, J. W. Bao, J. N. Wei, and T. J. Zhao. Chloride resistance of strain hardening cementitious composites under the artificially simulated marine tidal zone. *Journal of Building Materials*, Vol. 24, 2021, pp. 1–6 + 21.

[24] Li, J., Z. W. Wang, C. W. Yan, and S. G. Liu. Influence of temperature on chloride coefficient of polyvinyl alcohol fiber reinforced cementitious composites in chloride environment. *Concrete*, Vol. 318, 2016, pp. 36–38.

[25] Qin, Y., X. W. Zhang, J. R. Chai, Z. G. Xu, and S. Y. Li. Experimental study of compressive behavior of polypropylene-fiber-reinforced and polypropylene-fiber-fabric-reinforced concrete. *Construction and Building Materials*, Vol. 194, 2019, pp. 216–225.

[26] Murthy, A. R. and P. Ganesh. Effect of steel fibres and nano silica on fracture properties of medium strength concrete. *Advances in Concrete Construction*, Vol. 7, 2019, pp. 143–150.

[27] Liu, F. Y., W. Q. Ding, and Y. F. Qiao. Experimental investigation on the flexural behavior of hybrid steel-PVA fiber reinforced concrete

containing fly ash and slag powder. *Construction and Building Materials*, Vol. 228, 2019, id. 116706.
[28] Hari, R. and K. M. Mini. Mechanical and durability properties of basalt-steel wool hybrid fibre reinforced pervious concrete – A box Behnken approach. *Journal of Building Engineering*, Vol. 70, 2023, id. 106307.
[29] Hu, D., Q. G. Fu, L. Zhou, B. Liu, and J. Sun. Crack development behavior in thermally sprayed anti-oxidation coating under repeated thermal-oxygen coupling environment. *Ceramics International*, Vol. 47, 2021, pp. 15328–15336.
[30] Rostami, R., M. Zarrebini, K. H. Sanginabadi, D. Mostofinejad, S. M. Abtahi, and H. Fashandi. An investigation into influence of physical and chemical surface modification of macro-polypropylene fibers on properties of cementitious composites. *Construction and Building Materials*, Vol. 244, 2020, id. 118340.
[31] Pakravan, H. R., M. Latifi, and M. Jamshidi. Ductility improvement of cementitious composites reinforced with polyvinyl alcohol-polypropylene hybrid fibers. *Journal of Industrial Textiles*, Vol. 45, 2016, pp. 637–651.
[32] Algin, Z. and M. Ozen. The properties of chopped basalt fibre reinforced self-compacting concrete. *Construction and Building Materials*, Vol. 186, 2018, pp. 678–685.
[33] Ramesh, B. and S. Eswari. Mechanical behaviour of basalt fibre reinforced concrete: An experimental study. *Materials Today: Proceedings*, Vol. 43, 2021, pp. 2317–2322.
[34] Zheng, Y. X., J. B. Zhuo, P. Zhang, and M. Ma. Mechanical properties and meso-microscopic mechanism of basalt fiber-reinforced recycled aggregate concrete. *Journal of Cleaner Production*, Vol. 370, 2022, id. 133555.
[35] Zhang, P., C. Y. Wang, C. L. Wu, Y. F. Guo, Y. Li, and J. J. Guo. A review on the properties of concrete reinforced with recycled steel fiber from waste tires. *Reviews on Advanced Materials Science*, Vol. 61, 2022, pp. 276–291.
[36] Rehman, S. K. U., S. Kumarova, S. Ali Memon, M. F. Javed, and M. Jameel. A Review of microscale, rheological, mechanical, thermo-electrical and piezoresistive properties of graphene based cement composite. *Nanomaterials*, Vol. 10, 2020, id. 2076.
[37] Aslam, F., F. Farooq, M. N. Amin, K. Khan, A. Waheed, A. Akbar, et al. Applications of gene expression programming for estimating compressive strength of high-strength concrete. *Advances in Civil Engineering*, Vol. 2020, 2020, pp. 1–23.
[38] Li, V. C., S. X. Wang, and C. Wu. Tensile strain-hardening behavior of polyvinyl alcohol engineered cementitious composite (PVA-ECC). *ACI Materials Journal*, Vol. 98, 2001, pp. 483–492.
[39] Wang, L., S. H. Zhou, Y. Shi, S. W. Tang, and E. Chen. Effect of silica fume and PVA fiber on the abrasion resistance and volume stability of concrete. *Composites Part B: Engineering*, Vol. 130, 2017, pp. 28–37.
[40] Yang, Y., B. Chen, Y. Chen, F. Liu, X. Xie, W. Guo, and H. Wang. Effect of admixtures and PVA fiber on the mechanical properties of high strength cementitious grout. *Case Studies in Construction Materials*, Vol. 18, 2023, id. e01884.
[41] Wang, J. Q., Q. L. Dai, R. Z. Si, and S. C. Guo. Investigation of properties and performances of Polyvinyl Alcohol (PVA) fiber-reinforced rubber concrete. *Construction and Building Materials*, Vol. 193, 2018, pp. 631–642.
[42] Zhang, P., Q. Li, and Z. Sun. Effect of polypropylene fiber on durability of concrete composite containing fly ash and silica fume. *Composites Part B: Engineering*, Vol. 45, 2013, pp. 1587–1594.
[43] Karahan, O. and C. D. Atiş. The durability properties of polypropylene fiber reinforced fly ash concrete. *Materials & Design*, Vol. 32, 2011, pp. 1044–1049.
[44] Long, W. J., H. D. Li, L. Mei, W. W. Li, F. Xing, and K. H. Khayat. Damping characteristics of PVA fiber-reinforced cementitious composite containing high-volume fly ash under frequency-temperature coupling effects. *Cement and Concrete Composites*, Vol. 118, 2021, id. 103911.
[45] Ling, Y. F., P. Zhang, J. Wang, and Y. Z. Chen. Effect of PVA fiber on mechanical properties of cementitious composite with and without nano-SiO2. *Construction and Building Materials*, Vol. 229, 2019, id. 117068.
[46] JGJ/T 70-2009. *Standard for test method of basic properties of construction mortar [in Chinese]*. China Architecture and Building Press, Beijing, China, 2009.
[47] GBT50082-2009. *Standard for test methods of long-term performance and durability of ordinary concrete [in Chinese]*. China Architecture and Building Press, Beijing, China, 2009.
[48] Liu, L. L., S. L. Gao, J. D. Xin, and D. H. Huang. Effect of low-stress fatigue on the off-crack-plane fracture energy in engineered cementitious composites. *Advances in Civil Engineering*, Vol. 2018, 2018, pp. 1–9.
[49] Aygörmez, Y., O. Canpolat, M. M. Al-mashhadani, and M. Uysal. Elevated temperature, freezing-thawing and wetting-drying effects on polypropylene fiber reinforced metakaolin based geopolymer composites. *Construction and Building Materials*, Vol. 235, 2020, id. 117502.
[50] Zhang, P., C. Wang, F. Wang, and P. Yuan. Influence of sodium silicate to precursor ratio on mechanical properties and durability of the metakaolin/fly ash alkali-activated sustainable mortar using manufactured sand. *Reviews on Advanced Materials Science*, Vol. 62, 2023, id. 20220330.
[51] Zhang, P., X. Y. Sun, F. Wang, and J. Wang. Mechanical properties and durability of geopolymer recycled aggregate concrete: A review. *Polymers*, Vol. 15, 2023, id. 615.
[52] Zhang, C., J. Wang, W. D. Song, and J. X. Fu. Effect of waste glass powder on pore structure, mechanical properties and microstructure of cemented tailings backfill. *Construction and Building Materials*, Vol. 365, 2023, id. 130062.
[53] Li, H. D., Q. Zeng, and S. L. Xu. Effect of pore shape on the thermal conductivity of partially saturated cement-based porous composites. *Cement and Concrete Composites*, Vol. 81, 2017, pp. 87–96.
[54] Zhang, P., S. Y. Wei, J. J. Wu, Y. Zhang, and Y. Zheng. Investigation of mechanical properties of PVA fiber-reinforced cementitious composites under the coupling effect of wet-thermal and chloride salt environment. *Case Studies in Construction Materials*, Vol. 17, 2022, id. e01325.
[55] Gao, S. L. and Q. Wang. Effect of low temperature and moisture on bond properties of PVA fibres and engineered cementitious composite matrix. *Advances in Cement Research*, Vol. 35, 2023, pp. 26–38.
[56] Shen, Y. N., Q. H. Li, B. T. Huang, X. Liu, and S. L. Xu. Effects of PVA fibers on microstructures and hydration products of cementitious composites with and without fly ash. *Construction and Building Materials*, Vol. 360, 2022, id. 129533.
[57] Pakravan, H. R. and T. Ozbakkaloglu. Synthetic fibers for cementitious composites: A critical and in-depth review of recent advances. *Construction and Building Materials*, Vol. 207, 2019, pp. 491–518.

[58] Golewski, G. L. Fracture performance of cementitious composites based on quaternary blended cements. *Materials*, Vol. 15, 2022, id. 6023.
[59] Wang, Z. B., P. Sun, Y. D. Hu, and S. Han. Crack morphology tailoring and permeability prediction of polyvinyl alcohol -steel hybrid fiber engineered cementitious composites. *Journal of Cleaner Production*, Vol. 383, 2023, id. 135335.
[60] Zhang, P., X. Han, Y. X. Zheng, J. Y. Wan and D. Hui. Effect of PVA fiber on mechanical properties of fly ash-based geopolymer concrete. *Reviews on Advanced Materials Science*, Vol. 60, 2021, pp. 418–437.
[61] Zhang, P., Q. F. Li, J. Wang, Y. Shi, Y. X. Zheng, and Y. F. Ling. Effect of nano-particle on durability of polyvinyl alcohol fiber reinforced cementitious composite. *Science of Advanced Materials*, Vol. 12, 2020, pp. 249–262.
[62] Ren, J. G. and Y. M. Lai. Study on the durability and failure mechanism of concrete modified with nanoparticles and polypropylene fiber under freeze-thaw cycles and sulfate attack. *Cold Regions Science and Technology*, Vol. 188, 2021, id. 103301.
[63] Ma, H. Q., C. Yi, and C. Wu. Review and outlook on durability of engineered cementitious composite (ECC). *Construction and Building Materials*, Vol. 287, 2021, id. 122719.
[64] Yang, Y. K., R. A. Patel, S. V. Churakov, N. I. Prasianakis, G. Kosakowski, and M. Wang. Multiscale modeling of ion diffusion in cement paste: Electrical double layer effects. *Cement and Concrete Composites*, Vol. 96, 2019, pp. 55–65.
[65] He, F., C. Shi, X. Hu, R. Wang, Z. Shi, Q. Li, et al. Calculation of chloride ion concentration in expressed pore solution of cement-based materials exposed to a chloride salt solution. *Cement and Concrete Research*, Vol. 89, 2016, pp. 168–176.
[66] Zhang, T. W. and O. E. Gjørv. Effect of ionic interaction in migration testing of chloride diffusivity in concrete. *Cement and Concrete Research*, Vol. 25, 1995, pp. 1535–1542.
[67] Li, V. C., H. Stang, and H. Krenchel. Micromechanics of crack bridging in fiber-reinforced concrete. *Materials and Structures*, Vol. 26, 1993, pp. 486–494.
[68] Wang, Z. Y., X. W. Liang, and T. W. Zhai. Predicting the flexural behavior of steel-PVA hybrid fiber reinforced cementitious composite. *Structures*, Vol. 51, 2023, pp. 1189–1204.
[69] Tawfek, A. M., Z. Ge, H. Yuan, N. Zhang, H. Zhang, Y. Ling, et al. Influence of fiber orientation on the mechanical responses of engineering cementitious composite (ECC) under various loading conditions. *Journal of Building Engineering*, Vol. 63, 2023, id. 105518.
[70] Liu, S. G., S. Lu, L. Q. Yin, C. W. Yan, L. H. Lu, and J. Zhou. Mechanical strength model of engineered cementitious composites with freeze–thaw damage based on pore structure evolution. *Cement and Concrete Composites*, Vol. 134, 2022, id. 104706.
[71] Öztürk, O. Comparison of frost resistance for the fiber reinforced geopolymer and cementitious composites. *Materials Today: Proceedings*, Vol. 65, 2022, pp. 1504–1510.
[72] Nam, J., G. Kim, B. Lee, R. Hasegawa, and Y. Hama. Frost resistance of polyvinyl alcohol fiber and polypropylene fiber reinforced cementitious composites under freeze thaw cycling. *Composites Part B: Engineering*, Vol. 90, 2016, pp. 241–250.